Desalination and Water Treatment
www.deswater.com

doi: 10.5004/dwt.2021.27379

229 (2021) 314–321
July

Catalytic oxidation of polymer used in oilfield by bentonite supported Cu(II) complexes in a wide pH range

Liwa Ma[a], Yuying Xue[a], Weichao Du[a], Jie Zhang[a,b], Chengtun Qu[a,b,*], Gang Chen[a,b,*]

[a]*Shaanxi Province Key Laboratory of Environmental Pollution Control and Reservoir Protection Technology of Oilfields, Xi'an Shiyou University, Xi'an 710065, China, emails: xianquct@xsyu.edu.cn (C. Qu), gangchen@xsyu.edu.cn (G. Chen), 1755464919@qq.com (L. Ma), 958362272@qq.com (Y. Xue), duweichao@xsyu.edu.cn (W. Du), zhangjie@xsyu.edu.cn (J. Zhang)*

[b]*State Key Laboratory of Petroleum Pollution Control, CNPC Research Institute of Safety and Environmental Technology, Beijing 102206, China*

Received 26 June 2020; Accepted 18 April 2021

ABSTRACT

Currently, the treatment of organic pollution in oilfield-produced water has been increasingly considered. In this work, a catalyst of sodium citrate-Cu(II) complex supported on bentonite (B) (B@Cu(II)L) was prepared to appraise its capacity of catalytic degrading for hydroxypropyl guar gum (HPGG), polyacrylamide (PAM), and carboxymethyl cellulose (CMC) in oilfield wastewater. Significant effect parameters considered of diverse temperature, H_2O_2 concentration, B@Cu(II)L dosage, and pH value in heterogeneous Fenton-like course were investigated, respectively. The results show that B@Cu(II)L exhibits high catalytic performance for the degradation of HPGG in a wide pH range of 7.0–13.0. The viscosity of HPGG can be reduced effectively with the 20.0% H_2O_2 (mass ratio to HPGG) and 10.0% B@Cu(II)L (mass ratio to H_2O_2). The removal rate for chemical oxygen demand (COD) of HPGG, PAM, and CMC reaches to 96.1%, 94.1%, and 95.0%, respectively, within 240 min under the optimized conditions, and the COD of an oilfield wastewater sample can be removed by 93.0% under the same condition.

Keywords: Bentonite supported complex; Clean oxidation; Produced water; Oil field

1. Introduction

There is a large amount of oilfield-produced wastewater as the oil and gas fields are continuously exploited [1,2]. Produced water is a toxic and complex mixture of organic dispersed and inorganic salts and dissolved oil, etc., which may cause bioaccumulation and toxicity for marine animals [3]. Polymer flooding technology is widely used in oil recovery, and contamination has been a highly urgent environmental issue in oil and gas fields [2,4]. At present, hydroxypropyl guar gum (HPGG), with a structure of biodegradable and biocompatible heteropolysaccharide composed of a β-(1–4) D-mannopyranose backbone linked with α-(1–6) D-galactopyranose units [5,6], has been widely used as an oilfield fracturing additive because of the high viscosity of its aqueous solutions at low concentrations [7–9]. Therefore, there is a large amount of HPGG in the produced water after fracturing, which needs to be treated due to its high viscosity, serious corrosion to facilities, and potential risks to the health of the residents around the oilfield. So far, the treatment of wastewater can be roughly divided into physical, chemical, and biological methods according to the principle of treatment methods [10,11]. Physical processes of adsorption on activated carbon can remove both organic and inorganic compounds [12,13]. Nevertheless, they have high costs, transferring contaminants from one phase to another and producing solid waste, but the management is another drawback of this method [14]. Biological treatment is a

* Corresponding author.

cost-effective and environmentally friendly alternative with higher efficiency [15]. However, the sensitivity of the microorganisms to the toxicity and variation of organic chemicals in produced water limits its field application [16,17]. Therefore, Fenton oxidation and its modification have been widely employed in some studies to treat oilfield wastewater, and Fenton-like methods have drawn much attention of many researchers recently [18–20].

The Fenton reagent reacts with organic compounds complicated composition and difficult to degrade in an aqueous solution by strong oxidizing hydroxyl radicals generated from the reaction of Fe^{2+} and hydrogen peroxide (H_2O_2). Finally, a large number of organic molecules convert to some small molecules, such as carbon dioxide (CO_2) and water (H_2O) [20,21]. Unfortunately, it is restricted to a low and narrow pH range of 2.0–3.0 to ensure the Fenton reagent working effectively, so the procedures of application are cumbersome, and the range of application is finite [22,23]. In recent years, there have been numerous studies on expanding the pH range of the Fenton system, but there are still some disadvantages such as high cost, limited pH range, and no practical application in the oil fields [24,25]. Thus, we seek an efficient Fenton oxidation processing for the treatment in the oilfield wastewater at a wide pH range.

In this work, the main attempt was devoted to partially destroy HPGG contained in oilfield-produced water and improve the degradability of the wastewater through the oxidation of metal-hydrogen peroxide (H_2O_2) in a wide pH range. In this study, the heterogeneous catalyst of B@Cu(II)L was determined for the Fenton oxidation. The catalyst was measured for degradation performance to the viscosity of HPGG and the chemical oxygen demand (COD). Besides, the catalyst was applied to the oilfield wastewater. The experimental conditions of Fenton oxidation were optimized and the B@Cu(II)L was thoroughly characterized by scanning electron microscopy (SEM), X-ray diffraction (XRD), X-ray photoelectron spectroscopy (XPS), inductively coupled plasma-mass-spectrometry (ICPMS), Fourier-transform infrared (FT-IR), and N_2 adsorption–desorption isotherms.

2. Materials and methods

2.1. Chemicals and materials

Commercial calcium bentonite (B) was obtained from Fengyun Chemical Co., Ltd., Xi'an, China, sodium citrate, $CuCl_2{\cdot}2H_2O$, NaOH, H_2O_2 (30%), $KMnO_4$, $K_2Cr_2O_7$, $FeSO_4$, $(NH_4)_2Fe(SO_4)_2{\cdot}6H_2O$, HPGG, polyacrylamide (PAM), and carboxymethyl cellulose (CMC) (purity > 95%) were obtained from Xinhe Environmental Protection Co., (Zhengzhou, China). Instrument of measuring automatically for kinematic viscosity of petroleum products (SYD-265 H) was purchased from Benshan Instrument Equipment Co., Shanghai, China. Ubbelohde viscometer was purchased from Shenyi Glass Co., Shanghai, China.

2.2. Catalyst preparation

The complex of Cu(II)L was prepared by blending 1.71 g $CuCl_2{\cdot}2H_2O$ and the ligand solution (L) of 2.94 g sodium citrate with the ratio of 1:1 (molar ratio) in a flask under stirring at room temperature for 2 h. The synthesis process of Cu(II)L complex was exhibited in Fig. 1.

And then the B@Cu(II)L was prepared according to the following Eq. (1):

$$\mathrm{Cu(II)L} + \mathrm{bentonite(B)} \rightarrow \mathrm{B@Cu(II)L} \quad (1)$$

5.5 g bentonite (B), dried at 80°C for 24 h before the experiment, was added to the solution achieved above, and stirred for 4 h under 60°C. Then the solid sample was centrifuged at 3,000 rpm and washed twice with 20 mL distilled water. Finally, the supported catalyst (B@Cu(II)L) was obtained after dried at 70°C overnight.

2.3. Catalyst characterization

B and B@Cu(II)L were characterized by various characterization methods. The morphology and elemental composition analysis of heterogeneous catalysts were obtained with powdered samples by means of a field emission SEM (JSM-6390A). The phase composition and purity of the catalyst were analyzed by powder XRD on an XRD-6000 diffractometer using Cu Kα radiation at 40 kV voltage and 15 mA current. XPS measurements were carried out on ESCALAB250Xi electron spectrometer using 300 W Al Kα radiations. All IR measurements were performed on an FT-IR spectrometer at room temperature at the range from 400 to 4,000 cm^{-1}. N_2 adsorption–desorption isotherms were performed on a Micrometrics ASAP 2020 HD88 instrument at 77 K, for which the samples were degassed at 300°C for 4 h before the measurement. The surface areas were calculated using the Brunauer–Emmett–Teller (BET) equation in the pressure of range P/P_0 = 0.02–0.2, and the pore size distribution was calculated using the Barrett–Joyner–Halenda (BJH) method. The percentage of copper leached was analyzed by ICPMS. Finally, the total organic carbon (TOC)

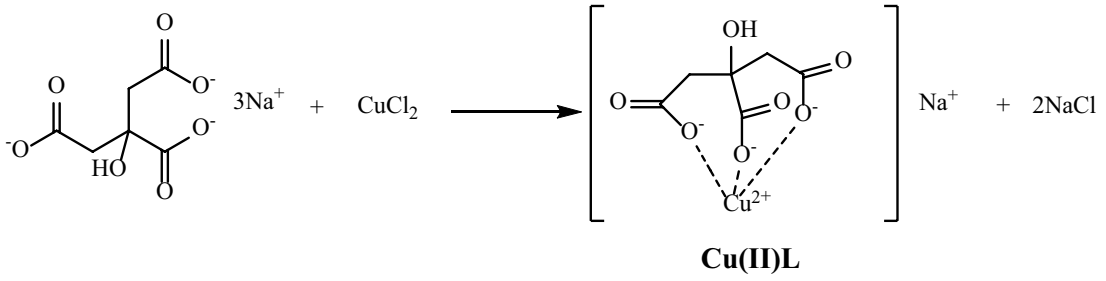

Fig. 1. Synthesis of Cu(II)L complex.

analysis was conducted to evaluate the performance of the catalyst.

2.4. Degradation process

HPGG was dispersed in distilled water at room temperature and stirred 30 min under a magnetic stirrer with a stirring rate of 100 rpm for 12 h to complete the swelling. Appropriate amounts of HPGG solution, hydrogen peroxide (H_2O_2), and B@Cu(II)L were sequentially added into the Ubbelohde viscometer. The dosage of the HPGG (0.6%) was 5 mL, the mass of the hydrogen peroxide was 10% of the mass of the HPGG, and the dosage of the metal complex of the B@Cu(II)L was 10% of the mass of the hydrogen peroxide (H_2O_2). Then distilled water (5 mL) was added into the solution and mixed evenly, and the pH was adjusted by NaOH [26,27]. In this work, the kinematic viscosity value was evaluated automatically at 0, 5, 10, 15, 20, 25, 30, 35, and 40 min at a definite temperature [28]. Significant parameters considered for diverse temperature, H_2O_2 concentration, B@Cu(II)L dosage, and pH value in heterogeneous Fenton-like course were, respectively, evaluated by the method of the control variable. The COD of the HPGG, PAM, and CMC degradation before and after were measured according to the Chinese National Standard-GB11914, and the removal rate was calculated in detail according to Eq. (2). The wastewater produced in the oilfield was diluted appropriately before the experiment and tested according to the Chinese National Standard-GB11914:

$$\text{Removal rate of COD}(\%) = \frac{\left(\text{COD}_{t_0} - \text{COD}_t\right)}{\text{COD}_{t_0}} \times 100\% \quad (2)$$

where COD_{t_0} and COD_t are COD values at the initial and t times, respectively.

3. Results and discussion

3.1. Characterizations of catalyst

B@Cu(II)L is a complex generated from the reaction of sodium citrate and copper chloride and then loaded on bentonite (B). The morphology of B@Cu(II)L was characterized by SEM scanned of ×1,000 and ×5,000 at first. As exhibited in Fig. 2, the SEM of bentonite and B@Cu(II)L indicates the morphology of the supported copper-based complex has no significant change in the two bentonite samples.

In addition, the phase composition of the catalyst was analyzed by powder XRD. As exhibited in Fig. 3, the peaks are mainly corresponding to SiO_2 marked by Q [29]. Compared with B, the overall peak is weaker. According to the 2θ from 5° to 10°, there is basically no change, indicating that the complex is only supported on the surface of the clay. It is observed that the diffraction peaks at 2θ = 35.18° and 61.76° (JCPDS79-0988) are assigned to copper oxide [30], which indicates the loading of copper-based complex Cu(II)L over bentonite.

XPS can be used for the chemical composition of the sample [31]. Therefore, B and B@Cu(II)L were characterized by XPS technology. Compared with B, as shown in Fig. 4, the new binding energy peak that appeared at 930–950 eV can be assigned to copper, which indicates the presence of copper supported on the bentonite [32].

Meanwhile, B and B@Cu(II)L were analyzed by infrared spectrum, as exhibited in Fig. 5. The band at 1,035.9 cm^{-1} is attributed to the bending vibrations and is

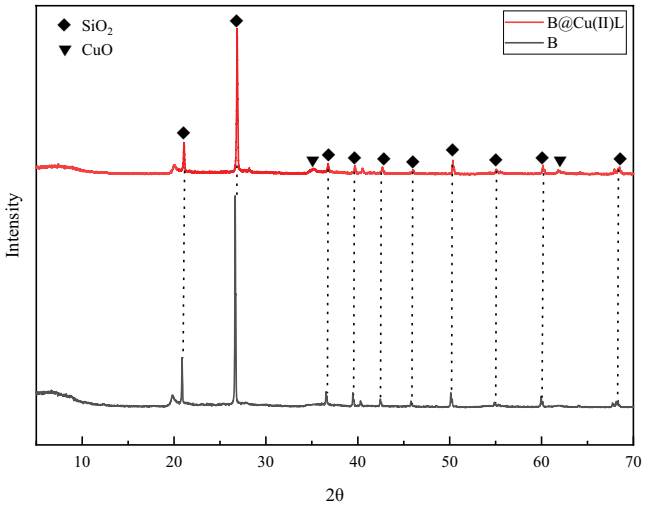

Fig. 3. XRD pattern of B and B@Cu(II)L.

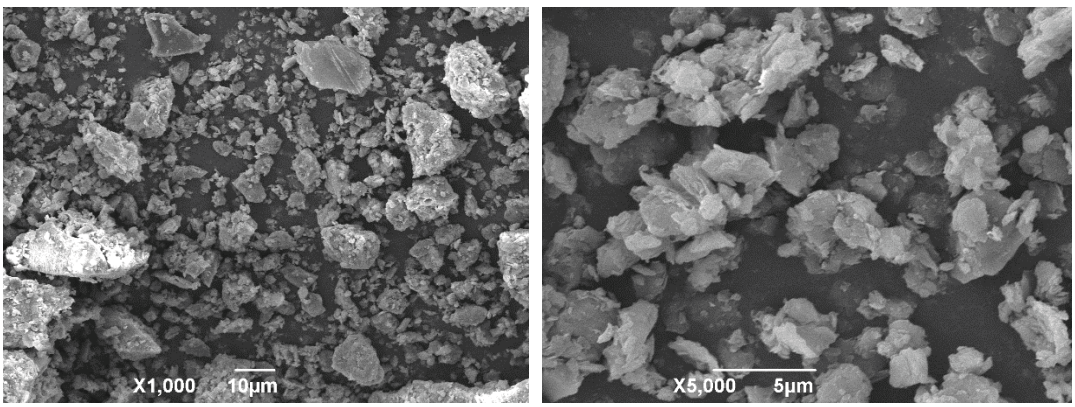

Fig. 2. SEM of B@Cu(II)L.

closely related to the stretching vibrations of Si–O–Si and the stretching vibrations of C–C, and the peak at 530.3 cm^{-1} was due to O–Si–O bending vibration [33,34]. The band at 1,604.41 cm^{-1} is corresponding to the C=O stretching vibrations [35], and the peak at 3,457.1 cm^{-1} is due to O–H bond stretching vibrations [36]. Compared with B, the new peaks at 1,439.6 and 1,399.0 cm^{-1} are due to $–CH_2$ deformation vibrations [36]. Therefore, it is obvious that the Cu(II)L complex has loaded on bentonite.

In the meanwhile, the porosity of B@Cu(II)L was investigated and calculated according to Eq. (3) listed below. Results show that the adsorption capacity of B@Cu(II)L is 61.33 mg/g. What's more, the N_2 adsorption–desorption isotherms of B and B@Cu(II)L was gained by the method of BET. The surface areas, pore volumes, and pore size of B and B@Cu(II)L were showed in Table 1, and the N_2 adsorption–desorption isotherm of B@Cu(II)L is an IV isotherm, and has an H_3-type hysteresis loop ($P/P_0 > 0.4$), as exhibited in Fig. 6. It demonstrates that there are micropores, and B@Cu(II)L has uniform pores of a narrow size. Besides, H_3-type hysteresis indicates the most prevalent plate-like particle in slit-shaped pores [37]. Compared with B, the overall quantity adsorbed of B@Cu(II)L increases, and combined with Table 1, it can be obtained that the pore size, pore-volume, and surface area increase. Therefore, it can be concluded that B@Cu(II)L has a high adsorption capacity, which may contribute to high catalytic capacity in the degradation potential of organic polymers:

$$q_e = \frac{(C_0 - C_t)V}{m} \tag{3}$$

where q_e (mg/g) is the adsorption capacity of B@Cu(II)L, C_0 (mg/L) and C_t (mg/L) are the concentration of HPGG in solution at initial and t (min) times, respectively. V (L) is the total volume of HPGG solution, m (mg) is the adsorbent of B@Cu(II)L mass.

Finally, in order to know the percentage of copper leached, the washing water was analyzed by ICPMS (Inductively coupled plasma mass spectrom). Results exhibit a load of copper is 0.57 g/g, which further illustrates the copper has loaded on bentonite and supports previous XRD and N_2 adsorption–desorption.

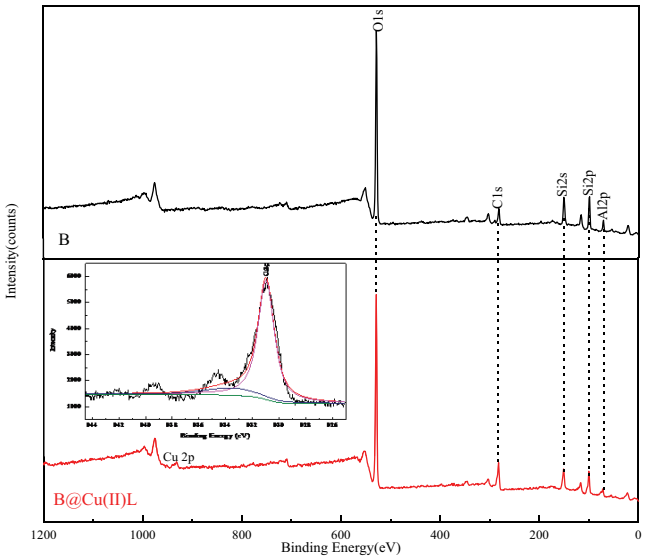

Fig. 4. XPS spectra of B and B@Cu(II)L.

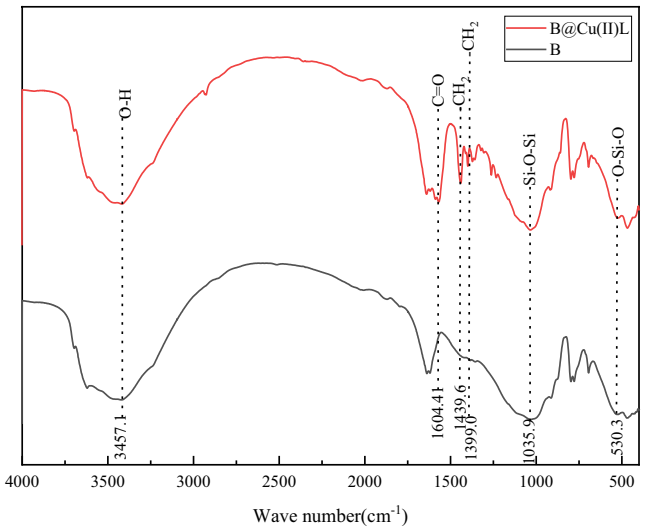

Fig. 5. FT-IR spectra of B and B@Cu(II)L.

Table 1
Pore properties of B and B@Cu(II)L

	B	B@Cu(II)L
Pore size (nm)	5.2310	6.0957
Pore volume (cm^3/g)	0.0946	0.1237
Surface area (cm^2/g)	70.6773	76.7528

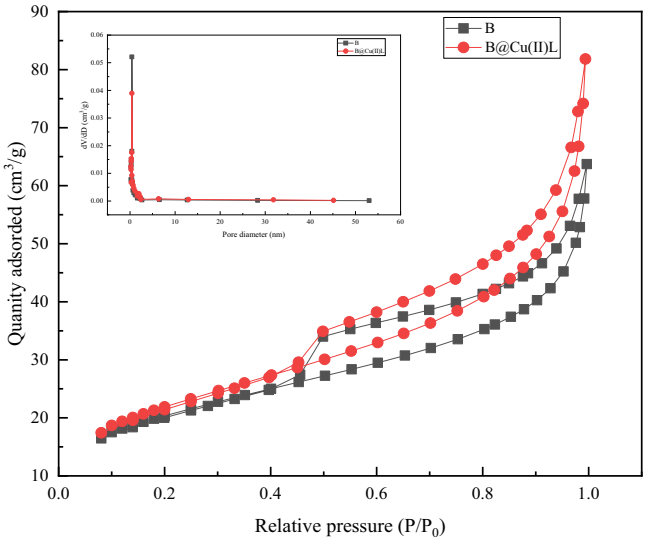

Fig. 6. Nitrogen adsorption–desorption isotherms and pore size distribution of B and B@Cu(II)L.

3.2. Effect of temperature

As we know, hydrogen peroxide can be activated to produce $HO^{\bullet}$ by using a transition metal as a catalyst [37]. The catalytic performance of in the presence of B@Cu(II)L to catalysis the degrade HPGG can be evaluated by the relative viscosity due to HPGG degradated into small molecular, which causes the viscosity of the solution to decrease, because the viscosity of the solution greatly depends on the extent of HPGG degradation. The catalytic mechanism can be described as the following equations [37,38]:

$$Cu^{2+} + H_2O_2 \rightarrow Cu^{+} + HO_2^{\bullet} + H^{+} \quad (4)$$

$$HO_2^{\bullet} \leftrightarrow O_2^{-\bullet} + H^{+} \quad (5)$$

$$Cu^{2+} + O_2^{-\bullet} \leftrightarrow Cu^{+} + O_2 \quad (6)$$

$$Cu^{2+} + HO_2^{\bullet} \leftrightarrow Cu^{+} + O_2 + H^{+} \quad (7)$$

$$Cu^{2+} + H_2O_2 \rightarrow Cu^{2+} + HO^{\bullet} + OH^{-} \quad (8)$$

The temperature represents a crucial parameter and plays a significant role in the oxidation process on degradation efficiency of polymers. The influence of reaction temperature on the degradation performance for HPGG was investigated at 25°C, 30°C, 35°C, 40°C, and 45°C respectively using B@Cu(II)L as a catalyst with 10.0% H_2O_2 (mass ratio to HPGG) and 10.0% B@Cu(II)L (mass ratio to H_2O_2) at pH 7.0. The obtained results in Fig. 7 demonstrate that the degradation is obviously influenced by the reaction temperature. The viscosity of HPGG significantly decreases within 5 min and then keeps a continuously tardy decrease degradation rate. Temperature affects the viscosity reduction obviously below 40°C, while it is not further effective as it above 40°C. As expected, the viscosity of HPGG can be decreased from 22.00 to 1.33 mm²/s within 40 min at 45°C. It is obviously obtained that the oxidation degradation is an endothermal reaction, and a higher reaction temperature can benefit the degradation, which is consistent with the previously studied results [35–38]. Thus, concerning the application and the efficiency, a reaction temperature of 45°C was chosen as the optimum temperature for the following experiments.

3.3. Effect of catalyst dosage

The degradation process is influenced by catalyst dosage, so the dosage of catalyst was increased from 1 to 20% (mass ratio to H_2O_2) to choose the optimal dosage of B@Cu(II)L at 45°C, pH 7.0, and 10% H_2O_2 (mass ratio to HPGG). Generally speaking, the degradation of polymers should be more effective as the amount of catalyst increases. However, a large amount of catalysts is not always useful for the degradation process. Fig. 8 confirms that the viscosity of the HPGG solution is significantly influenced by the catalyst dosage. Obviously, the viscosity of HPGG significantly decreased when the B@Cu(II)L dosage increased from 1 to 10% due to the increasing amount of active sites for H_2O_2 decomposition, and the lowest viscosity value decreased to 1.33 mm²/s in 40 min in the presence of 10% B@Cu(II)L. However, the efficiency decreases as the dosage of catalyst increases to 20%. It is because that the degradation efficiency is low and the polymer is not degraded thoroughly when the dosage of catalyst is low. Besides, the capillary will be blocked resulting in the increase of viscosity, when the catalyst dosage is high. Therefore, 10% was chosen as the optimal catalyst dosage in the following study.

3.4. Effect of H_2O_2 concentration

In order to evaluate the effect of H_2O_2 concentrations on the degradation process in the presence of B@Cu(II)L,

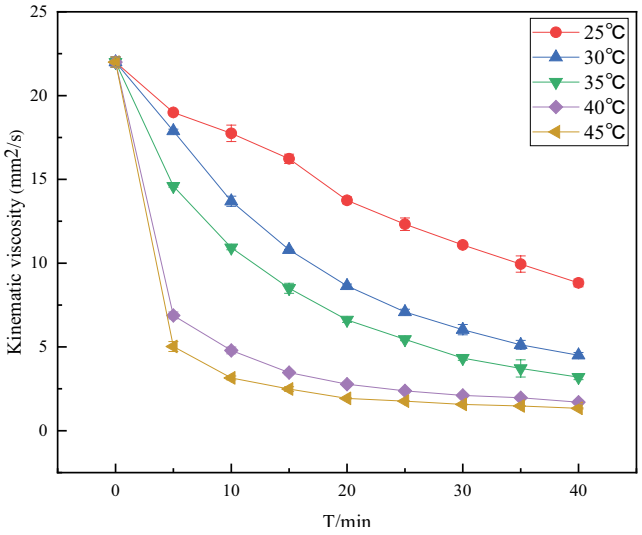

Fig. 7. Effect of reaction temperature (10.0% H_2O_2, 10.0% B@Cu(II)L, and pH 7.0).

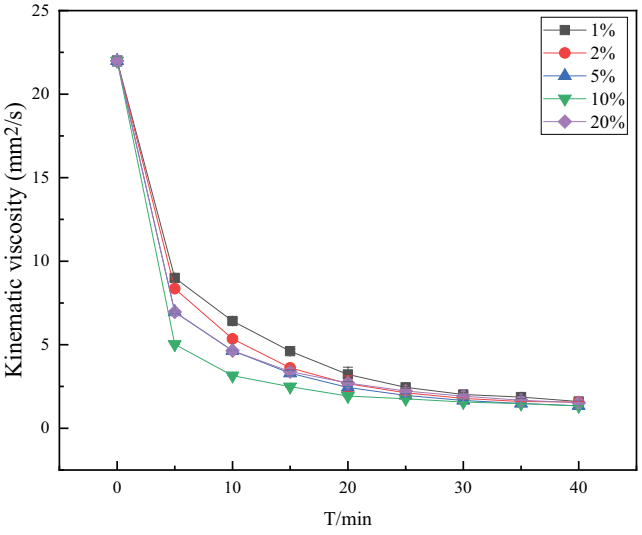

Fig. 8. Effect of B@Cu(II)L dosage (10.0% H_2O_2, 45°C, and pH 7.0).

the effect of H_2O_2 was investigated by varying its concentration from 1 to 30% (mass ratio to HPGG) catalyzed by 10% B@Cu(II)L (mass ratio to H_2O_2) at 45°C and pH 7.0. The result was exhibited in Fig. 9, and it can be observed that the viscosity of HPGG is significantly influenced by the concentration of H_2O_2. The viscosity of HPGG significantly decreases within 5 min and then keeps a continuously tardy decline degradation rate. The degradation performance increases with the increasing H_2O_2 from 1% to 25% due to more radicals formed. However, an evident improvement is not found under a higher concentration (30%). It is because hydroxyl radicals scavenging effect resulting in performance drop-down under an excessive hydrogen peroxide [35–38]:

$$H_2O_2 + HO^{\bullet} \rightarrow H_2O + HO_2^{\bullet} \quad (9)$$

Fig. 8 also evidences that the effect of H_2O_2 concentrations 25% and 20% almost equal. Considering the economic principles and degradation efficiency, 20% was selected as the optimum H_2O_2 concentration.

3.5. Effect of pH

The conventional Fenton oxidation with H_2O_2–Fe^{2+} has rigorous requirements on the acidity and alkalinity of the oilfield wastewater due to the hydration transformation of Fe^{2+} to $Fe(OH)_2$ under a high pH value [38]. Consequently, pH should be adjusted to acidic conditions in most processing methods used in the treatment of these wastewaters. The influence of pH on the Fenton process has been studied in previous investigations, and it was founded to be specifically significant. In order to investigate the effect of pH on this Fenton like process, the degradation of HPGG was conducted at diverse pH of 7.0, 9.0, 10.0, 12.0, 13.0, and 14.0, respectively, in the presence of 10% B@Cu(II)L (mass ratio to H_2O_2) and 20% H_2O_2 (mass ratio to HPGG) at 45°C and pH 7.0. In this work, the pH was adjusted with NaOH, and the results were presented in Fig. 10. It illustrates that the degradation of HPGG can be performed quite effectively under alkaline conditions, which were even better than that in the neutral condition. The highest degradation efficiency was observed in the presence of B@Cu(II)L at pH 12.0, and the viscosity of HPGG can be decreased to 0.74 mm^2/s within 40 min. Thus, pH 12.0 was selected as the optimal pH under considering the economic principles and degradation performance. In addition, it can be obtained that the B@Cu(II)L can effectively broaden the application of Fenton processing with an extensive pH range of 7.0–14.0.

3.6. COD removal

COD is considered a significant parameter in evaluating and monitoring water quality. HPGG, CMC, and PAM, as thickeners, are commonly used in oilfields [38]. Therefore, the three polymers were used to evaluate the catalytic oxidation performance of catalysts on COD removal. Three polymers with a mass concentration of 0.6% were, respectively, oxidized by enough H_2O_2 at 45°C and pH 12, and the results are shown in Figs. 11 and 12. It is observed obviously that the COD of three polymers significantly decreased within 40 min, and the removal rate, respectively, reaches 72.6%, 63.9%, and 51.2%. The removal rate increases to 96.1%, 95.0%, and 94.1% within 240 min under the same conditions. Besides, the removal rate TOC of HPGG, CMC, and PAM can reach 99.8%, 99.3%, and 99.6%. Thus, the results demonstrate that B@Cu(II)L has high catalytic performance on the oxidation of multifarious polymers.

3.7. Application in oilfield wastewater processing

The B@Cu(II)L was applied to process a Changqing Oilfield produced wastewater sample (the wastewater is clear and no suspended solids, with a pH of 8, which has been deeply treated) based on the optimized reaction condition to further evaluate its catalytic oxidation performance.

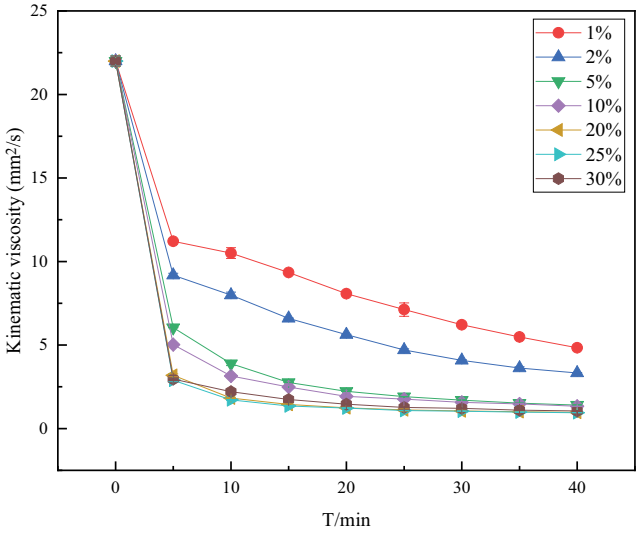

Fig. 9. Effect of H_2O_2 concentration (10.0% B@Cu(II)L, 45°C, and pH 7.0).

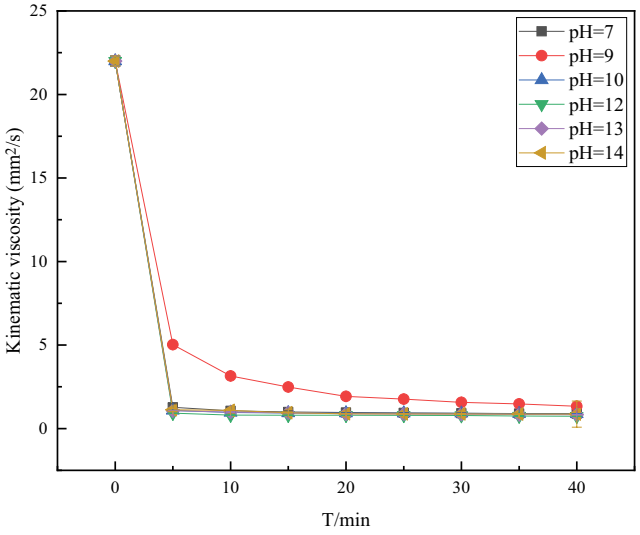

Fig. 10. Effect of pH (20.0% H_2O_2, 10.0% B@Cu(II)L, 45°C, and pH 7.0).

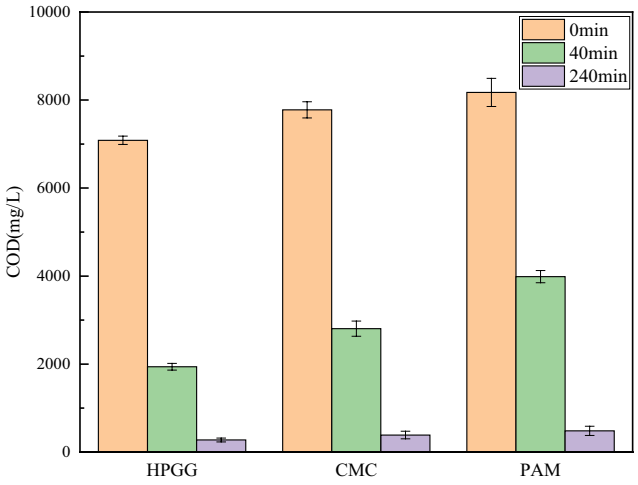

Fig. 11. COD degradation of diverse polymers (enough H_2O_2, 10.0% B@Cu(II)L, 45°C, and pH 12.0).

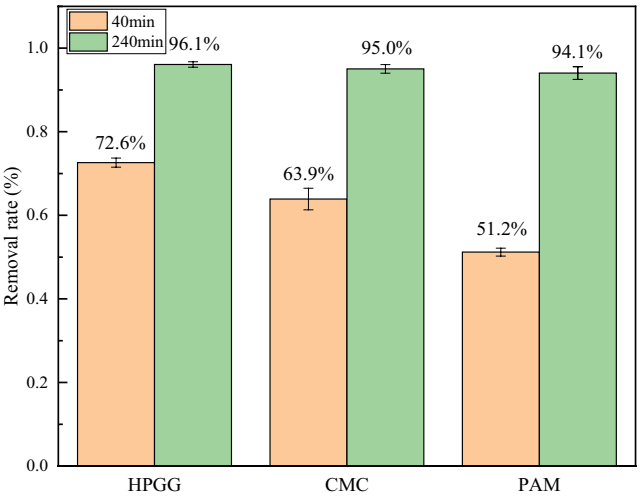

Fig. 12. Removal rate of diverse reaction time (enough H_2O_2, 10.0% B@Cu(II)L, 45°C, and pH 12.0).

The COD removal experiments were carried out in this pretreated produced wastewater, and the results are exhibited in Fig. 13. As expected, B@Cu(II)L has high efficiency to remove the COD of the water sample. COD values decrease from 4,336.2 to 1,740.32 mg/L within 40 min, and the removal rate reaches 59.9%. The removal rate can reach to 93.0% within 240 min under the optimized conditions. The result illustrates that the catalyst can catalyze clean oxidation on the degradation of the oilfield produced wastewater effectively.

4. Conclusions

In this paper, B@Cu(II)L of citrate-Cu(II) complex supported on bentonite (B) as catalyst was prepared for Fenton-like oxidation under high pH value. The B@Cu(II)L was used for the degradation of HPGG, and the optimum experimental conditions were selected by significant parameters considered for various temperatures, pH value, catalyst dosage, and oxidizing agent of hydrogen peroxide concentration in

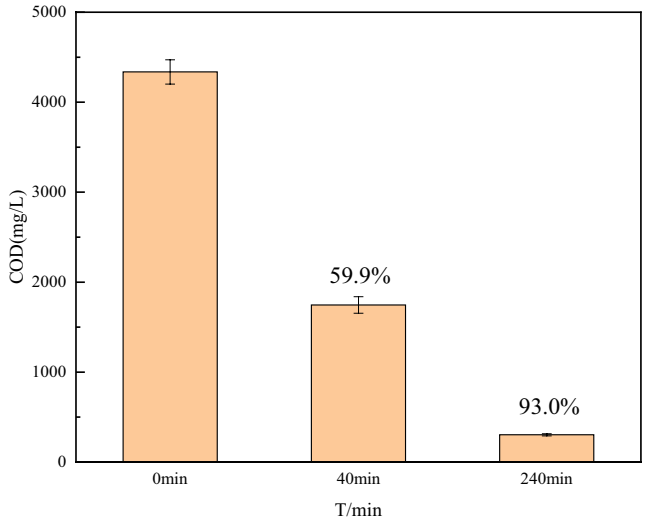

Fig. 13. Application in the processing of oilfield wastewater (enough H_2O_2, 10.0% B@Cu(II)L, 45°C, and pH 12.0).

the heterogeneous degradation process. The consequences indicate that B@Cu(II)L performs high performance for the degradation of HPGG in a wide pH of 7.0–14.0, and viscosity of HPGG can be effectively reduced at 45°C with 10% B@Cu(II)L (mass ratio to H_2O_2) and 10% H_2O_2 (mass ratio to HPGG). The COD removal rate of HPGG, PAM, and CMC can be significantly increased within 240 min at a high pH value up to 12. The removal rate of oilfield produced wastewater can reach to 93.0% under adequate H_2O_2 within 240 min in the presence of B@Cu(II)L, which further illustrates that the catalyst can catalyze the clean oxidation on the degradation of the oilfield produced wastewater. The results will benefit the research work in the related field.

Acknowledgments

The work was supported financially by the Youth Innovation Team of Shaanxi University, Shaanxi Provincial Key Research and Development Program (2019ZDLGY06-03), and the Postgraduate Innovation Fund Project of Xi'an Shiyou University (YCS20211011). And we thank the work of the Modern Analysis and Testing Center of Xi'an Shiyou University.

References

[1] V. Sinha, S. Chakma, Advances in the preparation of hydrogel for wastewater treatment: a concise review, J. Environ. Chem. Eng., 7 (2019) 2213–3437.
[2] D. Zhao, C. Su, G. Liu, Y.B. Zhu, Z.Y. Gu, Performance and autopsy of nanofiltration membranes at an oil-field wastewater desalination plant, Environ. Sci. Pollut. Res. Int., 26 (2019) 2681–2690.
[3] S. Jiménez, M. Andreozzi, M.M. Micó, M.G. Álvarez, S. Contreras, Produced water treatment by advanced oxidation processes, Sci.Total Environ., 666 (2019) 12–21.
[4] S.W. Wang, Z.W. Li, Q.L. Yu, Kinetic degradation of guar gum in oilfield wastewater by photo-Fenton process, Water Sci. Technol., 75 (2016) 11–19.
[5] L.R.S. Moreira, E.X.F. Filho, An overview of mannan structure and mannan-degrading enzyme systems, Appl. Microbiol. Biotechnol., 79 (2008) 165–78.

[6] Y.C. Zhao, J.P. He, X.X. Han, X.L. Tian, M.Y. Deng, W.P. Chen, B. Jiang, Modification of hydroxypropyl guar gum with ethanolamine, Carbohydr. Polym., 90 (2012) 988–992.
[7] K. Yu, D. Wong, J. Parasrampuria, D. Friend, Guar Gum, H.G. Brittain, Ed., Analytical Profiles of Drug Substances and Excipients, Vol. 24, Academic Press, Murray Hill NJ, 1996, pp. 243–276.
[8] J.J. Patel, M. Karve, N.K. Patel, Guar gum: a versatile material for pharmaceutical industries, Int. J. Pharm. Pharm. Sci., 6 (2014) 13–19.
[9] N. Thombare, U. Jha, S. Mishra, M.Z. Siddiqui, Guar gum as a promising starting material for diverse applications: a review, Int. J. Biol. Macromol., 88 (2016) 361–372.
[10] P. Lv, X. Wang, Y. Chen, X. Guo, A. Xu, Z. Zhao, Optimization of chemical agents for removing dispersed oil from produced water in Z oilfield, Petrol. Sci. Technol., 35 (2017) 1285–89.
[11] D. Wang, D. Li, P. Lv, Y. Xu, Q. Wei, Deposition of polytetrafluoroethylene nanoparticles on graphene oxide/polyester fabrics for oil adsorption, Surf. Eng., 35 (2019) 426–434.
[12] Y. Sun, D. Wang, D.C.W. Tsang, L. Wang, Y.S. Ok, Y. Feng, A critical review of risks, characteristics, and treatment strategies for potentially toxic elements in wastewater from shale gas extraction, Environ. Int., 125 (2019) 452–469.
[13] Y. Sun, I.K.M. Yu, D.C.W. Tsang, X. Cao, D. Lin, L. Wang, N.J.D. Graham, D.S. Alessi, M. Komárek, Y.S. Ok, Y. Feng, X.-D. Li, Multifunctional iron-biochar composites for the removal of potentially toxic elements, inherent cations, and hetero-chloride from hydraulic fracturing wastewater, Environ. Int., 124 (2019) 521–532.
[14] S. Jiménez, M.M. Micó, M. Arnaldos, F. Medina, S. Contreras, State of the art of produced water treatment, Chemosphere, 192 (2018) 186–208.
[15] N. Lusinier, I. Seyssiecq, C. Sambusiti, M. Jacob, N. Lesage, N. Roche, Biological treatments of oilfield produced water: a comprehensive review, SPE J., 24 (2019) 2135–2147.
[16] A. Fakhru'l-Razi, A. Pendashteh, L.C. Abdullah, D.R.A. Biak, S.S. Madaeni, Z.Z. Abidin, Review of technologies for oil and gas produced water treatment, J. Hazard. Mater., 170 (2009) 530–551.
[17] N.N. Wang, T. Zheng, G.S. Zhang, P. Wang, A review on Fenton-like processes for organic wastewater treatment, J. Environ. Chem. Eng., 4 (2016) 762–787.
[18] Y. Gao, W.H. Zhu, Y.Q. Li, J.L. Li, S.N. Yun, T.L. Huang, Novel porous carbon felt cathode modified by cyclic voltammetric electrodeposited polypyrrole and anthraquinone 2-sulfonate for an efficient electro-Fenton process, Int. J. Hydrogen Energy, 46 (2021) 9707–9717.
[19] W.H. Zhu, Y.Q. Li, Y. Gao, C. Wang, J.F. Zhang, H.L. Bai, T.L. Huang, A new method to fabricate the cathode by cyclic voltammetric electrodeposition for electro-Fenton application, Electrochim. Acta, 349 (2020) 136415, doi: 10.1016/j.electacta.2020.136415.
[20] Y. Liu, Y. Zhao, J.L. Wang, Fenton/Fenton-like processes with in-situ production of hydrogen peroxide/hydroxyl radical for degradation of emerging contaminants: advances and prospects, J. Hazard. Mater., 4040 (2021) 124191, doi: 10.1016/j.jhazmat.2020.124191.
[21] M.A. Tony, Y.Q. Zhao, A.M. Tayeb, Exploitation of Fenton and Fenton-like reagents as alternative conditioners for alum sludge conditioning, J. Environ. Sci., 21 (2009) 101–105.
[22] S. Enami, Y. Sakamoto, A.J. Colussi, Fenton chemistry at aqueous interfaces, Proc. Natl. Acad. Sci. U.S.A., 111 (2014) 623–628.
[23] Y. Sun, Q.Y. Feng, X.D. Li, Application of response surface methodology to optimize degradation of polyacrylamide in aqueous solution using heterogeneous Fenton process, Desalination, 53 (2015) 1923–1932.
[24] X.F. Gu, F.L. Qin, G. Chen, Study on the synthesis of Fenton-like catalysts and their catalytic degradation properties of polyacrylamide, J. Environ. Pollut. Control, 34 (2012) 13–16.
[25] H. Gu, X. Tang, R.Y. Hong, Ubbelohde viscometer measurement of water-based Fe_3O_4 magnetic fluid prepared by coprecipitation, J. Magn. Magn. Mater., 348 (2013) 88–92.
[26] H.M. Aly, M.E. Moustafa, M.Y. Nassar, E.A. Abdelrahman, Synthesis and characterization of novel Cu(II) complexes with 3-substituted-4-amino-5-mercapto-1,2,4-triazole Schiff bases: a new route to CuO nanoparticles, J. Mol. Struct., 1086 (2015) 223–231.
[27] C.C. Su, M. Pukdee-Asa, C. Ratanatamskul, M.C. Lu, Effect of operating parameters on the decolorization and oxidation of textile wastewater by the fluidized-bed Fenton process, Sep. Purif. Technol., 83 (2011) 100–105.
[28] F. Zhu, L. Li, S. Ma, Z.F. Shang, Effect factors, kinetics and thermodynamics of remediation in the chromium contaminated soils by nanoscale zero valent Fe/Cu bimetallic particles, Chem. Eng. J., 302 (2016) 663–669.
[29] F. Tomul, Synthesis, characterization, and adsorption properties of Fe/Cr-pillared bentonites, Ind. Eng. Chem. Res., 50 (2011) 7228–7240.
[30] J.H. Ramirez, F.J. Maldonado-Hódar, A.F. Pérez-Cadenas, C. Monero-Castilla, C.A. Costa, L.M. Madeira, Azo-dye Orange II degradation by heterogeneous Fenton-like reaction using carbon-Fe catalysts, Appl. Catal., B, 75 (2007) 312–323.
[31] M. Slaný, Ľ. Jankovič, J. Madejová, Structural characterization of organo-montmorillonites prepared from a series of primary alkylamines salts: mid-IR and near-IR study, Appl. Clay Sci., 176 (2019) 11–20.
[32] P.F. Gao, X.Z. Long, Y. Xu, Study on the third generation polycarboxylic acid concrete water reducing agent, Appl. Chem. Ind., 49 (2020) 48–51.
[33] A.D. Bokare, W.Y. Choi, Review of iron-free Fenton-like systems for activating H_2O_2 in advanced oxidation processes, J. Hazard. Mater., 275 (2014) 121–135.
[34] A. Aguirrechu-Comerón, J. Pasán, J. González-Platas, J. Ferrando-Soria, R. Hernández-Molina, Halide copper(II) complexes of aromatic N-donor containing ligands: structural, magnetic and reactivity studies, J. Struct. Chem., 56 (2015) 1563–1571.
[35] M.V. Bagal, P.R. Gogate, Wastewater treatment using hybrid treatment schemes based on cavitation and Fenton chemistry: a review, Ultrason. Sonochem., 21 (2014) 1–14.
[36] M. Meng, J. Yang, X. Zhang, Y.J. Jia, L.W. Ma, Z.H. Ma, G. Chen, Y. Tang, Cysteine-Fe(III) catalyzed oxidation of common polymer used in oilfield by H_2O_2 in a wide pH range, Russ. J. Appl. Chem., 92 (2019) 135–140.
[37] Y. Tang, H. Liu, L. Zhou, H.M. Ren, H. Li, J. Zhang, G. Chen, C.T. Qu, Enhanced Fenton oxidation of hydroxypropyl guar gum catalyzed by EDTA-metal complexes in a wide pH range, Water Sci. Technol., 79 (2019) 1667–1674.
[38] Y. Tang, H.M. Ren, P.W. Yang, H. Li, J. Zhang, C.T. Qu, G. Chen, Treatment of fracturing fluid waste by Fenton reaction using transition metal complexes catalyzes oxidation of hydroxypropyl guar gum at high pH, Environ. Chem. Lett., 17 (2019) 559–564.